

NASA RASC-AL

2020 Moon to Mars Ice and Prospecting Challenge, Project Plan

Sub-lunar Tap-Yielding eXplorer, STYX

Team Members

All student members are undergraduate studying mechanical engineering at the California Polytechnic State University, San Luis Obispo. This team was formed on 10/9/2019 and volunteered to take on this challenge as part of a capstone project.

Chris Boone

- *Telemetry systems lead*

Aaron Erickson

- *Programming and electrical design lead*

Alex Krenitsky

- *Linear motion and drilling systems lead*

Ryan Locatelli

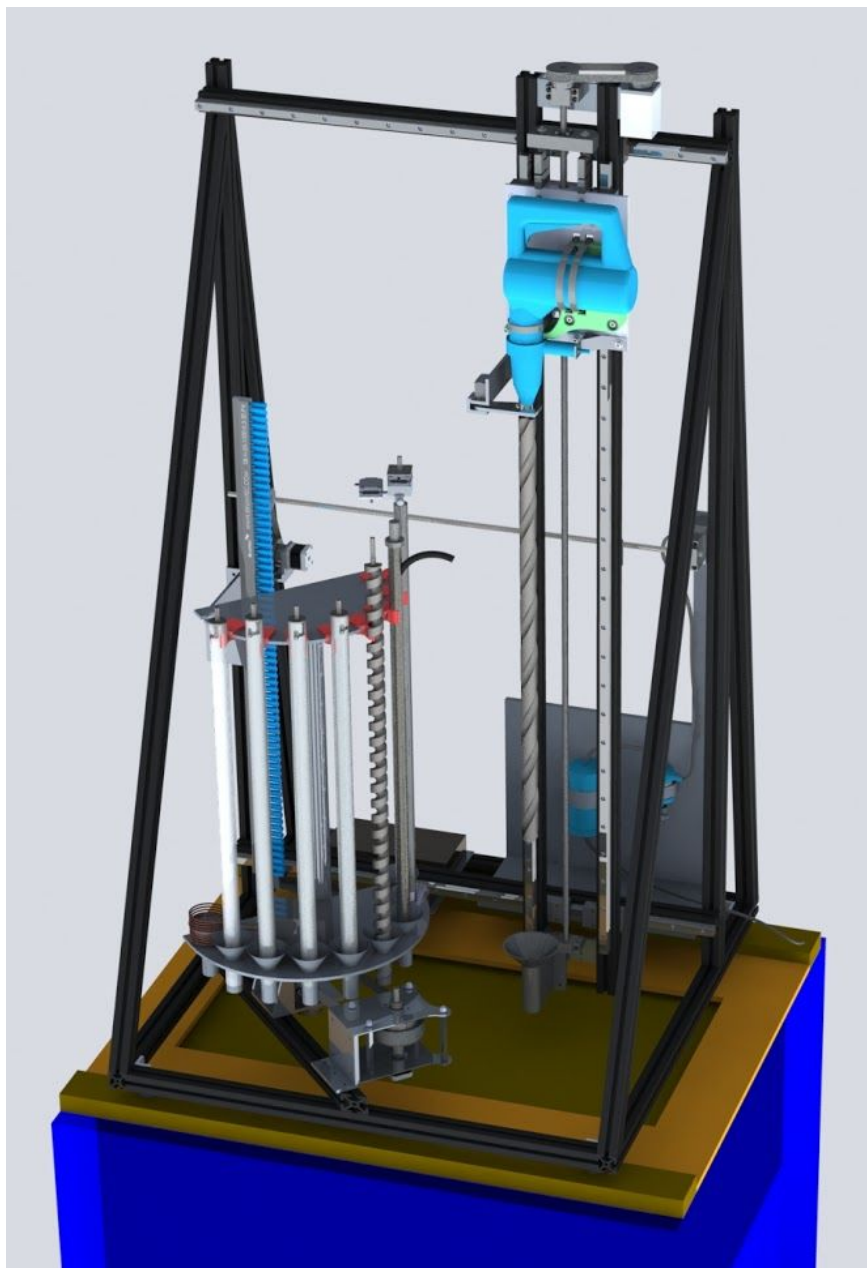
- *Water processing lead*

Westin McHaney

- *Thermal systems lead*

Dr. Peter Schuster

- *Faculty advisor*



CAL POLY

I. INTRODUCTION

The Sublunar Tap-Yielding eXplorer, STYX, is this team's proposed design for the 2020 NASA RASC-AL competition. The name STYX was chosen in reference to the mythological underground river that acts as a gateway to the underworld.

Design efforts toward the project have been focused on ideation, preliminary calculations, thorough CAD modeling, and concept model testing to ensure design feasibility. The results of these efforts are innovative and conceptually proven design choices that will differentiate STYX from other project proposals.

Some novel design features STYX will use are a rotary tool changer with swappable tools, a sleeve driving mode, a tool heater, and a pivoting heating probe. The STYX drill head will translate on two axes, use a rotary hammer drill to bore holes, sleeve boreholes with pipe to prevent collapse, and deliver water via a peristaltic pump and a two stage filtration system.

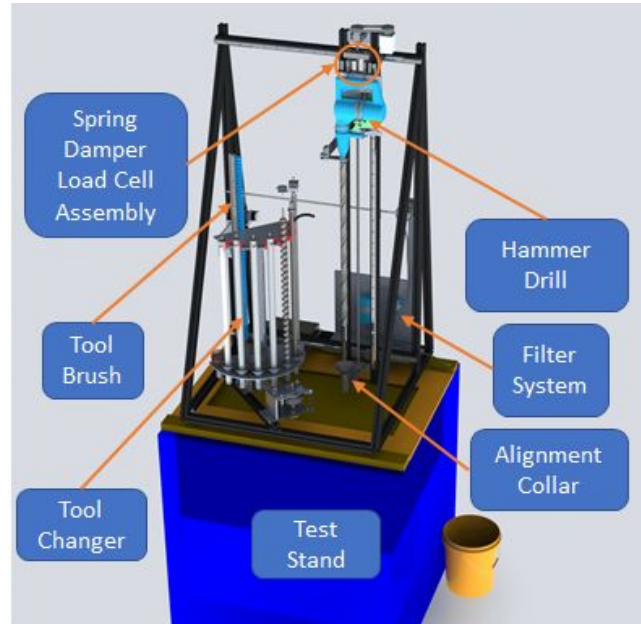


Figure 1. Annotated system overview

Linear Motion and Drilling Systems Lead: Alex Krenitsky works and teaches in Cal Poly's machine shop as a student technician and CNC operator, giving him experience with tight tolerancing and designing for manufacturability. He also has experience building 3D printers and designing small scale CNC milling machines. These projects show understanding of how to design and operate low-cost, high-rigidity machines. Finally, his work experience in Boeing's satellite mechanisms team will provide context for reliable and lightweight design.

Telemetry Systems Lead: Chris Boone has experience working with various telemetry systems, including one year of work with wildlife animal tracking systems, one year of work with telemetric avalanche beacons, and two summers of work at a radio frequency engineering company.

Programming and Electrical Design Lead: Aaron Erikson participated in high school robotics for four years and will provide the team with relevant Arduino and electrical control component experience. He is currently pursuing a mechatronics concentration and is taking classes on programming microcontrollers.

Water Processing Lead: Ryan Locatelli has hands-on experience with various water purification techniques from his work experience at a wastewater treatment facility. His experience will help to choose the appropriate sizing and methods for pumping and filtration.

Thermal Systems Lead: Westin McHaney has completed thermal system design classes via his major curriculum, providing him the tools to design the heating probe required for this design challenge. His analytical skills will produce a final design optimized for packaging and melt rate.

II. MECHANICAL DESIGN

The mechanical design is broken into six main subsystems: frame and lid Interface, linear motion, tool changer, heater probe actuation, and water processing.

A. Frame and Lid Interface

To interface with the provided 2x4 lengths mounted to the test bed lid, the horizontal base frame shown in Figure 1 will use angle brackets and a damping material spanning the width of the frame. ½" lag bolts installed every 6" will provide a mechanically secure, but vibrationally isolating mounting solution. A 1.5" square aluminum extrusion frame was chosen for its modularity and abundant interfacing methods. The outside dimensions of the frame will be just inside the 1m x 1m x 2m constraint to maximize machine travel.

B. Linear Motion

To move the drill head around the drillable envelope, the team chose a two-axis leadscrew configuration. While belt and ball-screw drives were considered, leadscrews can provide a desirable self-locking characteristic, significant mechanical advantage, and ample stiffness for the application. In the instance of an electrical fault, power outage or power-saving strategy involving the axis motors, the heavy drill head will remain passively supported by the lead screw. Preliminary torque, buckling, and mechanical resolution analyses were performed in MATLAB (Appendix A), and were used to justify this design choice and determine sizing. Two axis travel was chosen as a compromise between expanding the drillable area, reducing complexity, and retaining necessary rigidity for drilling operations. Styx will be capable of translating .8m in the horizontally and 1.4m vertically.

TPP23-240A10 stepper motors with current-controllable drivers were selected to power the lead screws based on their high degree of controllability, cost-effectiveness, and well-specified torque characteristics (TPP23 Stepper Motor). The motor's torque curve can be found in Appendix B. Travel speed, mechanical resolution, torque capacity, and power consumption were important factors considered while choosing motors.

A key feature of the Z-axis gantry is a spring-damper load cell interface, shown in Figure 2. Load cell data will provide closed-loop feedback to ensure that the 150N force on bit requirement is not exceeded. Plunging feed-rate will be adjusted via PID control. The integrated damper material will serve to reduce noise in the load cell data and vibratory loads to the leadscrew and frame. The compression springs will allow for greater resolution in force application, reduced shock loading to the leadscrew and frame, and compensation for feed rate in the event that the drill were to suddenly transition from a soft to a hard material. When the system is loaded in tension, the load is taken by rigid fasteners rather than springs.

HGH20 Linear rails were chosen to support the moment and shear loads during drilling operations (CNC Parts). While round profile linear bearings, roller-based systems, and sliding systems were considered, square profile rails had the highest load ratings for a given mass, best stiffness, and smallest packaging. Two rails and four HGH20CC carriages will be employed for each axis. Conservative free body diagram calculations completed in MATLAB (Appendix A) support the sizing choice for these rails. Finally, the alignment collar labeled in Figure 1 will constrain tools while plunging to minimize runout.

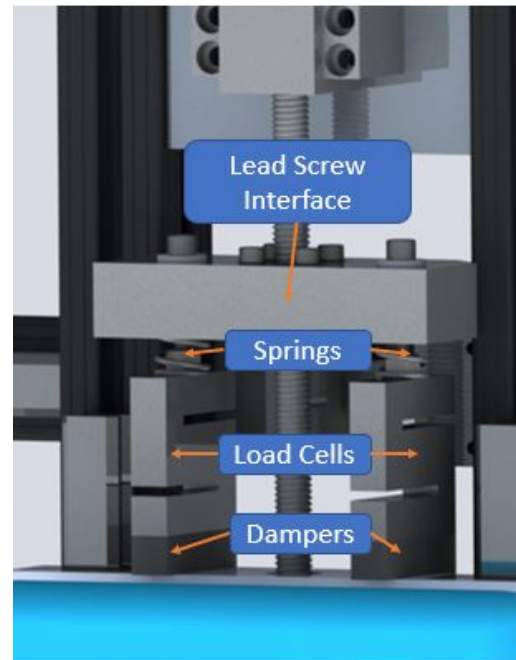


Figure 2. Load cell integration between Z-axis gantry and rotary the hammer drill.

C. Tool Changer

A main feature of STYX is the use of multiple tools, each with specialized tasks. To achieve this, a rotary tool changer was selected for its mechanical simplicity, compact footprint, and ability to add functionality to a single drill head. The rotary style tool changer shown in Figure 1 will support the needed tools while being able to rotate out of the drillable area. To change tools the drill gantry will jog to the correct coordinates, the tool rack will rotate to align a tool with the chuck, and a servo will actuate the drill's quick change mechanism.

D. Drilling Unit

For creating, clearing, and maintaining the holes necessary to reach ice, the team has decided to use a multi-function Bosch RH432VCQ rotary hammer drill with a quick change chuck (Bosch Power Tools). While alternative overburden penetration methods were investigated, including ultrasonic drilling, traditional drilling, and core-drilling, each of the alternatives had issues. Ultrasonic drilling is typically used for smaller diameter holes and is very expensive and complex to implement correctly. Traditional drilling in concrete applications suffers from slow penetration rates and poor drill bit life, especially with low axial forces. Finally, core-drilling is rarely used in dry applications with high length/depth ratios and would present additional tool cleaning challenges. Hammer drilling was chosen because abundant data is available on the topic, similar technology is already being used on interplanetary missions, and past teams have used hammer drills with great success.

The Bosch hammer drill chosen has multiple operating modes, including hammer drill, drill only, and hammer only, which will be selectable remotely via a servo. Forward and reverse directions are selectable as well. To achieve a borehole that is resistant to collapse and clear of debris, a 5-step, multi-tool process will be used, as highlighted in Table 1. This process requires tool changes, increasing system complexity, but reducing risk by allowing each tool to be optimized for a single task.

Table 1. 5-Step Drilling Process

Process/Tool	Drill Mode	Purpose
1.25" Masonry Drill	Hammer Drill	Break through all layers of overburden and 4" into the ice sheet.
1.25" OD, 1" ID Sleeve	Hammer Only	Drive a sleeve into the hole to prevent hole collapse, isolate chips for evacuation, and align/prevent dust ingress for the heater probe.
1" Auger	Drill Only	Clear out remaining material from inside the sleeve.
1" Heater Probe	Off	Melt 8" deep into ice and begin extraction. See section II part E and section III part A for additional detail.
Sleeve Extraction	Drill Only	Retrieval of sleeve for subsequent holes.

The masonry drill bit diameter was chosen from the following three factors; combination of extrapolated test data, required bore envelope for the heater probe, and the drill manufacturer's recommended maximum hole diameter in concrete. The test report in Appendix C shows that there was a roughly exponential trend between drill bit diameter and penetration rate. Extrapolating this trend gives an anticipated penetration rate of 1.6 in/minute using a 1.25" masonry drill in concrete.

Preliminary chip clearance testing with simulated overburden resulted in frequent hole collapse. 'Lessons learned' from previous years' competitions also identified chip evacuation and hole collapse to be a critical design issue. To address this common problem, a pile-driving solution was conceptualized and found to be extremely effective in small scale testing. In testing, documented in Appendix B, The hammering action of the drill provided enough force to drive a pipe into a pre-drilled hole, despite debris partially filling the hole. Remaining debris within the tube was then cleared with an auger. Based on this success, STYX will be moving forward with a reusable, bore-sleeving technique.

Finally, to reduce the effects of temperature on any drilling process, an induction heater coil capable of providing 1000W of heat will be mounted to the tool changer. At regular intervals, tools can be retracted from an in-progress hole and reheated to reduce the effects of freezing temperatures. Heating tools will also mitigate the risk of them becoming stuck or frozen in the overburden or ice. Keeping constant motion within the borehole, peck drilling to extract chips, and regularly cleaning tools off with the frame-mounted brush will also mitigate this risk. In the event that a tool does become stuck, it is anticipated that a hammer drilling action and up to 400N of upwards force will be enough to free any tool. Sizing of the vertical axis motor included consideration for this contingency.

E. Heater Probe Actuation

Another innovative design choice that STYX employs is a pivoting heater probe. Having a movable heating element maximizes the utility of each drilled hole. The heater probe shown in Figure 3 will be stored in the tool changer and mount to the drill chuck similar to the other tools used. The heating element will consist of three cartridge heaters and a thermistor encased within the pivoting copper housing. The drill head will actuate the heat probe vertically within the bore sleeve. One stepper motor will provide precise rotational control of the probe and another stepper motor will provide actuation of the pivot mechanism via a wire pulley system. These degrees of freedom provide a theoretical melt envelope of several stacked 8" diameter half-spheres, given a 4" heating element. While a large melt radius is desirable, 4" was deemed adequate and a higher watt density heating element will yield faster melt times while reducing stray heat transfer. Figure 3 depicts the heater yield at a single depth. An extraction tube extending to the bottom of the melt zone will interface with the pump system.

To reduce the risk of collapse, a 4" thick ceiling of ice will be left unmelted. Nonetheless, the pivot direction of the deployable heater element was chosen so that a hole collapse or tensile line failure would cause the mechanism to fail 'safe', meaning it could still be forcibly retracted from the hole. Additionally, the stepper motors driving the heater probe are sized to provide adequate torque under normal operating conditions, but will be incapable of driving the probe with enough force to damage it if the probe encounters significant resistance.

F. Pumping and Filtration

A peristaltic pump system with a self-cleanable, two-stage filter was selected for STYX. A two-stage filtration system allows for separate coarse and fine filter functions, protecting the finer stage

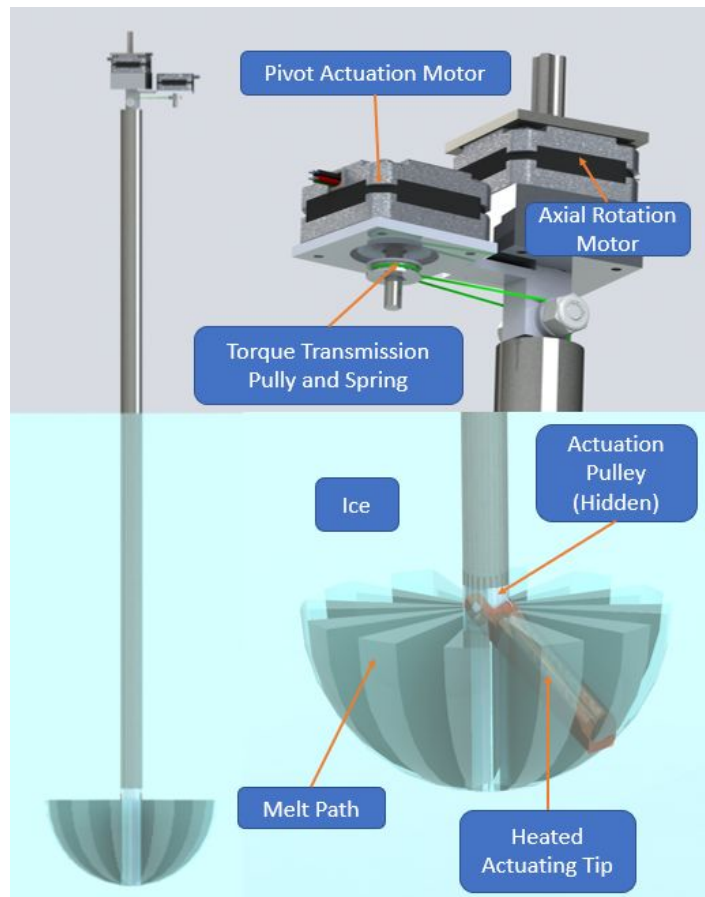


Figure 3. Left: Pivoting heater tool. Top right: Pivot and rotation stepper motors. Bottom right: Melt path of pivoting heater in ice.

from most of the fouling. The pump was chosen for its self-priming capability and its resilience to debris. Water will be pumped from the tip of the heater probe and into the first stage filter. Constant water pressure will feed the second filtration stage and flow into the collection bucket.

The first stage of the filtration system is a spin-down sediment trap designed to isolate large particulate. The sediment trap features a solenoid valve designed to periodically purge collected debris. An initial concept was 3D-printed and tested with moderate success. Final filter dimensions will be chosen based on real world ice melting rates, pump flow rate, and fouling characteristics.

The second stage of the filtration system relies on an extra-fine sintered stainless steel filter to remove particulates sized 5 microns and larger. This level of filtration should produce clear, potable water in the competition environment. An additional chemical filtration step would be needed on Mars to remove dissolved perchlorates. Sintered filters are physically strong, corrosion resistant, and backflow-able. Heat and vibration may be used to augment the backflow cleaning process. Heating causes the filter pores to expand, while vibration is effective for knocking particulate loose (Sintertech). This filter design and backflow strategy will minimize the required back pressure and flow velocity when cleaning the filter, ultimately preserving as much water as possible for collection.

Preliminary filter testing, documented in APPENDIX D, showed that tube blockage and sediment coagulation will be design hurdles. Tube blockage can occur when particles larger than .1" across enter the system. To prevent this, the heater probe tip will integrate a coarse, passive screen before the pump tube entrance. Testing verified the need for a multi-stage filter consideration to mitigate filter degradation from coagulating sediment. Because of this hands-on experience, the first-stage filter will be designed to operate under a fouled condition and will be optimized for thorough backflow. While the second stage filter will be as fine as possible.

III. ELECTRICAL DESIGN

The electrical control system for STYX will be based on a primary digital logic system with backup analog overrides available for all critical sub-systems. During normal operation, the Arduino will actuate AC components using solid state relays and DC components using Mosfets. Pulse-width modulated signals will be applied for the necessary components, along with the necessary shielding to prevent any electrical interference between components. During a fault situation, independent and redundant analog components can provide remote, manual control. An example circuit diagram is shown in Figure 4.

A. AC Components

When possible, components were designed to run natively on 120VAC to avoid voltage conversion losses. The heating element used in the heat probe is composed of three 120VAC, 2.5A cartridge heaters wired in parallel for a combined 7.5A current draw and 900W heating capacity. The Bosch drill chosen is rated for 8.5A at 120VAC.

B. DC Generation and Components

To convert AC to DC, STYX will utilize multiple switched-mode power supplies. A 1000W, 24VDC supply will power the high power stepper motors and induction coil heater. A 30W, 12VDC supply will

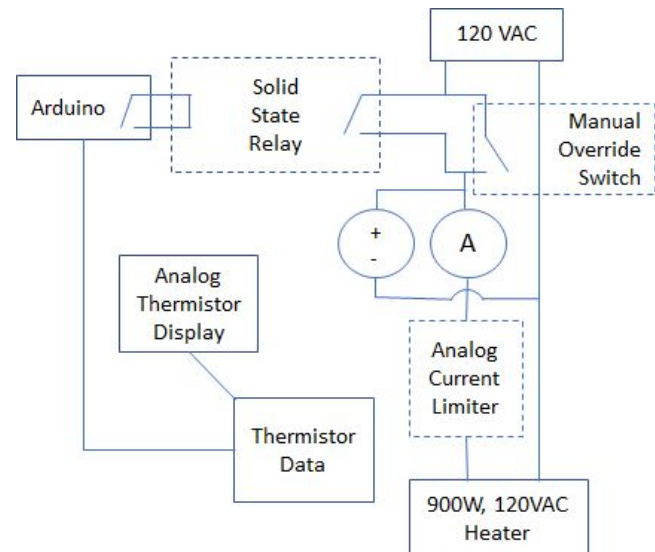


Figure 4. Heater circuit concept featuring redundant controls and analog overrides.

power the peristaltic pump and Arduino Mega. Finally, 2A, 5V supplies will provide power for on-board telemetry cameras, servos, low-power stepper motors, and other miscellaneous equipment.

C. Power Management

Using the required 9A fast blow fuse requires that current consumption be carefully monitored. The current curve for the Bussman BK/AGC-9-R model fuse, provided in Appendix E, shows some headroom above 9A for both starting current and continuous current. Current limiting may be used to mitigate start up loads and marginal continuous power modes. Standard operating procedures will be developed during testing. In addition, an Arduino controlled GUI will be implemented that prompts the operator before powering a component on if an over-current scenario is likely. Table 2 shows the anticipated load in different operating modes at the maximum and minimum expected line voltages. Component-level power draw is captured in APPENDIX F. DC components were conservatively assumed to have an AC/DC conversion efficiency of 85%.

Table 2. Power Budget Divisions

Operation	Components	Power (W)	Amps @ 120V	Amps @ 110V
Always On	Controls and Camera	27	0.23	0.25
Drilling	Z-Axis and Drill	1104	9.20	10.03
Drill bit Heating	Induction Heater	874	7.28	7.95
Melting and Extraction	Heater, Steppers A and B, Z-axis stepper, Pump	1033	8.61	9.39
Tool Change	X-axis, Z-axis, and A-axis steppers	152	1.26	1.38
Telemetry	Z-Axis Stepper	84	0.70	0.76

IV. SYSTEM CONTROL

The team intends to operate STYX in ‘hands-off’ mode for the entire duration of the competition. To do this, remote control systems with robust telemetry and some autonomous capability will be implemented. Whenever possible, digital control will be used with closed-loop PID controlled systems. The system stability for each operating mode will be thoroughly tested using both simulation and real world operation. In addition, programmed logic and status checks will prevent operational conflicts. To reduce the risk of a critical programming failure, each sub-system will also be operational in an open-loop, manual override mode. A graphical user interface (GUI) will provide the STYX operator with real-time system telemetry and prompts when system conditions approach operating limits.

A. Logic and Programming

Data logging, closed-loop operation, and the GUI will be managed via MATLAB’s Simulink. This Simulink model will control an Arduino Mega via serial interface. The Arduino will manage all component switching and analog data acquisition. Given the differences in available telemetry and risk associated with different operating modes, it is expected that drilling operations will be conducted autonomously, while tool changing and water extraction operations will be conducted remotely.

B. Telemetry

STYX will be capable of collecting temperature, power consumption, vertical force, water pressure, position and video telemetry. Some of these channels are solely to provide the operator with performance metrics, while others will be used to generate the required digital core.

To monitor performance metrics, thermocouple data will be collected from the heater probe tip and intermittent infrared temperature data will be collected from drilling tools. Electrical component temperatures may be monitored, but will also have integrated thermal protections. Power will be monitored at the system and component level via ammeters and voltmeters. Water flow rate data will

be used to monitor filtration and extraction rate. Positional data will be provided by stepper motor index. Finally, video telemetry will be used in a ‘telemetry probe’ for determining layer thickness and for monitoring tool changing operations.

Digital core creation will be split into two operations, layer thickness and hardness. To determine layer thickness, the telemetry probe will be inserted into a previously harvested hole. Unlike other borehole sleeves, this telemetry hole will utilize a clear, polycarbonate tube. A live video feed from the borehole, coupled with Z-axis position data will provide layer thickness data. Hardness data will be collected via force vs. feed rate data while drilling and a Brinell style hardness test. Load cell telemetry will be able to compare drilling force and rate to a list of previously tested materials. This type of telemetry can be collected during all drilling operations throughout the competition. For at least one hole, the telemetry probe will be used to measure force and deflection of each layer material using a Brinell style hardness test to produce another data set for comparison. This style of test will be especially useful on softer layers, where drilling data may have too much noise. If the drilling telemetry and probe telemetry agree, the layer’s compressive strength will be recorded. If not, the sample size will be increased.

V. TIMELINE

TABLE 3 highlights critical design, manufacturing, and test/integration milestones. A fully detailed Gantt chart is available in Appendix G. The schedule that the team has committed to was designed to leave approximately 4 weeks of margin between completion of full system stress testing and the competition’s full integration deadline of May 14th, 2019. This margin will be available in the instance that manufacturing or testing activities encounter issues.

Table 3. Project Milestones

Milestone	Date	Milestone	Date
Design Freeze	12/27/2019	Subsystem Testing Complete	2/12/2020
Purchasing Complete	1/1/2020	Full Integration Complete	2/28/2020
Subsystem Manufacturing Complete	2/4/2020	Full Stress Testing Complete	3/16/2020

VI. PATH TO FLIGHT

In addition to the usual design consideration of radiation, compatible materials, galling, off-gassing, and many other spacecraft design challenges, STYX would require several modifications to be fully operational in a lunar or martian environment. Some modifications will be made to the STYX testbed to be more representative of a real-world implementation.

A. Water Extraction on Mars

Mars has a thinner atmosphere than Earth with an average atmospheric pressure of 600 to 700 Pa, roughly 1% of Earth’s (Mars Education). This low atmospheric pressure paired with low surface temperatures, averaging at -81 ° Fahrenheit, results in sublimation of ice (Mars Facts). STYX’s martian ice extraction would be done by heating solid ice to assist in sublimation. Water vapor would be collected via the borehole sleeve, through which it would flow into a holding tank, where a cold plate would be used to refreeze the gas. To produce liquid water, the tank would occasionally be sealed and heated to obtain the necessary pressure and temperature to support liquid water. This process eliminates the need for pump-based extraction, filtration for particulates or dissolved perchlorates, and solves the issue of atmospheric pressure. Despite these numerous benefits, a slower yield rate than direct liquid extraction would need to be considered for mission planning.

Another consideration is the average surface temperature of Mars, -81 °F (Mars Facts). Because the bore sleeve is subjected to surrounding atmospheric, overburden, and ice temperatures, it is possible for water vapor to prematurely re-freeze within the sleeve, eventually blocking flow. To

overcome this problem, the bore sleeve would implement heating elements to maintain sublimation temperatures.

Finally, Styx's current design inserts and retracts rigid sleeves into each drilled hole to prevent hole collapse. STYX's sleeves will be 0.6 meters long, which is enough to confidently reach the ice layer given the known test bed layout. However, recent research has estimated that ice deposits would be at least 1 meter below the surface (Paradigm and Practicality). In order for STYX to be effective on Mars, the drilling, sleeving, and extraction operations need to reach deeper. Instead of expanding the frame and travel dimensions of the system, drilling and extraction systems could be implemented in a mole-style system demonstrated on the InSight mission, while sleeving is handled with a telescoping pipe (Sproewitz). Mole-style systems would only be limited by the length of cable available, which is lighter and more space-efficient than solid tools. A telescoping system, although more complex than rigid sleeves, would retain the reusability characteristic of the current sleeve design.

B. Prospecting on the Moon

The extreme temperature range of the lunar environment requires special consideration. Designing STYX to tolerate differential thermal expansion within assemblies and changing material properties would be critical. One example of a critical fit is between the brass lead screw nuts and stainless steel lead screws, as binding would occur with differential expansion. As temperature fluctuates, the changes in material property would require a recalibration of certain telemetry components such as load cells. Other components such as rubber belt drives would need to be replaced with more stable alternatives as rubber would become brittle or melt in lunar temperatures.

Lunar prospecting would only require drilling and telemetry systems, not extraction or purification systems. Additionally, mobility would be more highly valued for scientific purposes. To accommodate a mobile rover platform, extraneous systems would be removed to reduce weight and envelope. Additionally, adding a coring bit to the tool changer may be useful, since a central shaft is not required on every hole and core samples have more scientific value.

A critical consideration unique to the moon is dust ingress. The lunar surface is covered in a thin layer of highly abrasive, very fine particulate that has proven problematic since the Apollo program. To mitigate dust ingress, seals would be implemented at every moving interface, and the operational profile would be adjusted to reduced dust-producing activities. An example of this would be to use a 'drill only' mode rather than 'hammer drilling' whenever possible.

C. Testbed Enhancements

To better mimic martian and lunar operating conditions, vibration dampening will be integrated at the mounting points of STYX and between the drill assembly and the frame. Any non-terrestrial implementation would benefit from reduced vibratory loads.

Another necessary modification for lunar and martian readiness will be the sealing of all electrical control components within a Faraday cage to protect components from solar radiation. Grounding all electrical components will also be critical to prevent differential charging and mitigate the risk of arcing between equipment. STYX will be enclosing its on-board electronics in a sheet metal box and ensuring the entire system runs on a common ground connected to the provided 3-prong outlet.

VII. NOTE FROM THE TEAM

The STYX team is excited and proud to be presenting this design to NASA. Thank you for your time and the opportunity to participate in this competition. Cal Poly's College of Engineering and our enthusiastic faculty advisor have shown exceptional support for this project's success. We hope you find the presented design to be innovative and well-founded. We are eager to finalize, manufacture, test, and demonstrate our Sub-lunar Tap-Yielding Explorer design.

REFERENCES

Bussmann Series TDS for BK/AGC-9-R Fuse. Technical data 2543, May, 2017, <https://www.mouser.com/datasheet/2/87/eaton-agc-fast-acting-glass-tube-fuses-data-sheet-1608288.pdf>

“CNC Parts 20mm Linear Guide Rail 2pcs HGR20 L 1000mm Rail +4pcs HGH20CA HGH20CC \ Narrow Carriage Block.” *Aliexpress.com*

Jett, T, and K Street. *Lunar Dust Simulant in Mechanical Component Testing - Paradigm and Practicality*. NASA, ntrs.nasa.gov/archive/nasa/casi.ntrs.nasa.gov/20080015523.pdf.

“Mars Education: Developing the Next Generation of Explorers.” *Mars Education | Developing the Next Generation of Explorers*, marsed.asu.edu/mep/atmosphere.

“Mars Facts.” NASA, NASA, 27 July 2019, mars.nasa.gov/all-about-mars/facts/.

Martin Chaplin: “Water Phase Diagram.” *Water Phase Diagram*, www1.lsbu.ac.uk/water/water_phase_diagram.html

“PORAL, Sintered Metal Porous Filters.” *SINTERTECH*, sintertech.org/portfolio/poral-sintered-metal-porous-filters/.

“RH432VCQ 1-1/4 In. SDS-plus® Rotary Hammer with Quick-Change Chuck System.” | *Bosch Power Tools*, www.boschtools.com/us/en/boschtools-ocs/sds-plus-hammers-rh432vcq-34744-p/.

Sproewitz, Tom, et al. “HP3 Instrument Support System Structure Development for the NASA/JPL Mars Mission InSight.” 2019 IEEE Aerospace Conference, 2019, doi:10.1109/aero.2019.8742104.

“TPP23 Stepper Motor TorquePower™ Plus Series.” *ElectroCraft*, www.electrocrafter.com/products/stepper/TPP23/.

SEE APPENDIX J FOR ADDITIONAL BACKGROUND RESEARCH AND ASSOCIATED REFERENCES

APPENDIX A - MATLAB Preliminary Analysis

1

Contents

- CODE NOTES
- Drill Forces
- Z Ballscrew and motor calcs
- Z axis Leadscrew Calcs
- X Ballscrew and motor calcs
- X axis Leadscrew Calcs
- Y axis belt Calcs
- Heater Lifter Motor - AKA Axis B
- Heater Spring - ARCHIVED, NOT USED ANYMORE

```
% Alex Erenitsky
% Senior Project
% MATLAB 1
% Last Updated 11/3/2019
```

CODE NOTES

CODE IS MEANT TO BE RUN IN SECTIONS. FIND APPROPRIATE SECTION AND ONLY RUN THAT SECTION. NO VARIABLES ARE CARRIED BETWEEN SECTIONS.

```
clear all;
close all;
format short;
format compact;
clc;
```

Drill Forces

See drawing on Alex's page 27 of senior project notebook

```
clc;
clear all;
close all;
format short;
format compact;

r10=[5,-5,-36]; % Vector from R1 to drillbit tip
r2=[10,0,-7]; % Vector from second block to first block for M1 and M2
rba=[-10,0,0]; % Vector from second block to first block for M2
P=[20,20,35]; % Force Applied at Drillbit tip
M=[0,0,3.7*12]; % Moment applied at drillbit tip
M1=(-r10(2)*F(3)-r10(3)*F(2)+M(1),-(r10(1)*F(3)-r10(3)*F(1)+M(2),r10(1)*F(2)-r10(2)*F(1)+M(3));

% From M1(1)
Fyz2=-M1(1)/r21(3);
```

```
AMS_Tp=[num2str(Tp),'Nm'];
Tf=0; % Torque due to friction of support bearings, provided by manufacturer [Nm]
AMS_Tf=[num2str(Tf),'Nm'];
Tc=(C0*Vp^2)/RPM; % Total torque required at constant speed, [N-cm]
AMS_Tc=[num2str(Tc),'N-cm'];

% Acceleration forces
N=10; % RPM
ta=1; % Acceleration time [s]
Jm=0; % Inertia of motor, provided by manufacturer, [kg-m^2]
Jsh=0; % Inertia of screw shaft, provided by manufacturer [kg-m^2]
Jl=0; % Inertia of load [kg-m^2]

w_prime=(2*pi*N)/(60); % Angular acceleration
J_s=Jm+Jsh+Jl; % Inertia of system [kg-m^2]
Tacc=w_prime^2*J_s; % Torque ndue to acceleration [Nm]
Ta=Tacc+Tc; % Total torque during acceleration [Nm]
AMS_Ta=[num2str(Ta),'Nm'];

% COMPARE OUTPUTS TO TORQUE/SPEED/AMP CURVES PROVIDED AT ELECTRO-CRAFT.COM
% https://www.electrocraft.com/products/stepper/T9934/

steps_rev=200;
max_resolution=2/steps_rev % [mm]
```

```
Feed = 12.5000
RFS = 1.2500
AMS_Tc = 'Constant Speed Torque [Nm] =78.3042'
max_resolution = 0.0500
```

Z axis Leadscrew Calcs

```
clear all;
clc;
close all;
format short;
format compact;

F=50; % MAX Vertical load being reacted during drilling or lifting [lbf]
M=30; % Weight of entire z-axis gantry [lbf]
F=(F*M)*1.445; % TOTAL load converted Newton [N]
do=12; % Nominal (outer) diameter [mm]
p=2; % Pitch of screw
l=4; % Lead of screw [mm]
stars=1/p;
dr=do-1.299038*p; % Minor diameter of screw [mm]
da=(do+dr)/2; % Average diameter of screw [mm]
f=.25 % Friction coefficient. Lower is conservative if calculating min self-locking for
```

3

2

```
Fyrl=-(Fyz2+F(2));

% From M1(2)
Fxr2=M1(2)/r21(3);
Fxl=-(Fxr2+F(1));

% From M1(3)
Fyrb=M1(3)/rba(1);
Fyca=-(Fyrb+F(3));

FS=4;
PureMoment=M1*FS
R1=[Fxr1/2,Fyrl/2+Fyca/2,0]*FS
R2=[Fxr2/2,Fyz2/2+Fyca/2,0]*FS
R3=[Fxl/2,Fyrl/2+Fyrb/2,0]*FS
R4=[Fxr2/2,Fyrl/2+Fyrb/2,0]*FS
```

```
PureMoment =
    1.0e+03 *
    2.3800   -3.5800   0.9776
R1 =
   -295.7143   -216.8343    0
R2 =
    255.7143   134.5943    0
R3 =
   -295.7143   -244.5943    0
R4 =
    255.7143   106.8343    0
```

Z Ballscrew and motor calcs

```
%SOURCE: https://www.linear-motion-tips.com/calculate-motor-drive-torque-ball-screws/
clear all;
clc;
close all;
format short;
format compact;

F=50; % Force in z-axis desired [N]
m=20; % mass of entire z-axis gantry [kg]
g=9.8; % acceleration due to gravity [m/s^2]
mu=1; % Rail friction coefficient
FS=1.5; % z-axis factor of safety
Fa=F*m*g*mu; % Total force required for z-axis including FS [N]
P=10; % z axis ball screw lead [mm]
Feed=12.5 % min feedrate at max load [mm/sec]
RFS=Feed/P
etaNom=0.85; % Ball screw efficiency, nominal
etaRed=1; % Ball screw efficiency reduction, degradation due to dirt
eta=etaNom-etaRed; % z axis ball screw efficiency

Td=(Fa*P)/(2000*pi*eta); % torque to drive the load [Nm]
AMS_Td=[num2str(Td),'Nm'];
Tp=0; % Torque from nut preload, provided by manufacturer [Nm]
```

```
%
yatand(1/(pi*dm));
Lockcheck=and(y);
if fLockcheck
    disp('self-locking')
else disp('NOT self-locking')
end
FS=1.5; % FACTOR OF SAFETY
Tz=(F*dm)/2*((1+(pi*f*dm))/(pi*dm)-(f*1))/10*FS % Raising Torque (Not relevant in horis
ontal) [N-cm];
Tl=(F*dm)/2*((1-(pi*f*dm))/(pi*dm)+(f*1))/10*FS % Lowering Torque (Not relevant in hor
izontal) [N-cm];

steps_rev=200; % Motor characteristic
max_resolution=1/steps_rev % max resolution of screw [mm]
disp('mm')

f =
    0.2500
Lockcheck =
    0.1190
self-locking
Tr =
   108.6077
Tl =
    36.3358
max_resolution =
    0.0500
mm
```

X Ballscrew and motor calcs

```
%SOURCE: https://www.linear-motion-tips.com/calculate-motor-drive-torque-ball-screws/
clear all;
clc;
close all;
format short;
format compact;

F=50; % Force in axis desired [N]
m=20; % mass of entire axis gantry [kg]
g=9.8; % acceleration due to gravity [m/s^2]
mu=2; % Rail friction coefficient
FS=1.5; % z-axis factor of safety
Fa=F*m*g*mu; % Total force required for axis including FS [N]
P=10; % z axis ball screw lead [mm]
Feed=25 % min feedrate at max load [mm/sec]
RFS=Feed/P
etaNom=0.85; % Ball screw efficiency, nominal
etaRed=1; % Ball screw efficiency reduction, degradation due to dirt
eta=etaNom-etaRed; % z axis ball screw efficiency

Td=(Fa*P)/(2000*pi*eta); % torque to drive the load [Nm]
AMS_Td=[num2str(Td),'Nm'];
```

4

5

```

Tp=0; % Torque from nut preload, provided by manufacturer [Nm]
ANS_Tp=[num2str(Tp),'Nm'];
Tf=0; % Torque due to friction of support bearings, provided by manufac
turer [Nm]
ANS_Tf=[num2str(Tf),'Nm'];
Tc=(Td+Tp+Tf)*FS; % Total torque required at constant speed, [Nm]
ANS_Tc=[Constant Speed Torque [Nm] =',num2str(Tc)];

% Acceleration forces
Nm=10; % N/M
ta=1; % Acceleration time [s]
Jm=0; % Inertia of motor, provided by manufacturer, [kg-m^2]
Js=0; % Inertia of screw shaft, provided by manufacturer [kg-m^2]
Jl=0; % Inertia of load [kg-m^2]

w_prime=(2*pi*N)/(60*t); % Angular acceleration
Js=Js+JsJl; % Inertia of system [kg-m^2]
Tacc=Jw_prime; % Torque ndue to acceleration [Nm]
Ta=Ta+Tc; % Total torque during acceleration [Nm]
ANS_Ta=[Acceleration Torque [Nm] =',num2str(Ta)];

% COMPARE OUTPUTS TO TORQUE/SPEED/AMP CURVES PROVIDED AT ELECTROCRRAFT.COM
% https://www.electrocraft.com/products/stepper/TFP34/

steps_rev=200;
max_resolution=9/steps_rev % [mm]

Feed =
25
RPS =
2.5000
ANS_Tc =
Constant Speed Torque [Nm] =0.28393'
max_resolution =
0.0500
    
```

X axis Leadscrew Calcs

```

clear all;
clc;
close all;
format short;
format compact;

rail_fric=0.2 % Bearing Friction
N=90; % Entire x-axis carriage weight [lb]
Fw=rail_fric*4.448; % Convert Load to Newton [N]
do=12; % Nominal (outer) diameter [mm]
p=2; % Pitch of screw [mm]
l=4; % Lead of screw [mm]
start=L/p;
dr=do-1.299038*p; % Minor diameter of screw [mm]
da=(do+dr)/2; % Average diameter of screw [mm]
    
```

22.2000
N-cm

Heater Lifter Motor - AKA Axis B

```

clear all;
clc;
close all;
format short;
format compact;
% NOTES:
% 1 CORRESPONDS TO THE DRIVEN SHAFT INSIDE THE HEATER
% 2 CORRESPONDS TO THE DRIVER SHAFT, EITHER BEFORE OR AFTER GEARING. READ
% COMMENTS.
D1=5; % Effective diameter of pulley inside heater [in]
D2=3; % Effective diameter of pulley on driving motor [in]
R1=D1/2;
R2=D2/2;
COM=3; % COM distance from pivot point [in]
M=2; % Weight of pivot arm [lb]
Gearing=10; % Gear reduction from motor thru driver shaft
FSmotor=2; % FS of motor torque
Tmotor=(D2/D1)*M*COM*FSmotor/Gearing; % [in-lb]
Tmotor=Tmotor*11298*100 % Convert to N-cm
disp('N-cm');
N2=3; % RPS of motor shaft
N1=M/D1*N2/Gearing % RPS of driven shaft
deg_sec=N1*360 % Max Deployment speed [deg/sec]
    
```

Tmotor =
13.5576
N-cm
N1 =
0.0500
deg_sec =
18

Heater Spring - ARCHIVED, NOT USED ANYMORE

```

clear all;
clc;
close all;
format short;
format compact;

A=201e3; % for music wire, from table 10-4 [kpsi-in^3]
w=145; % for music wire, from table 10-4
d=.089; % Wire diameter, chosen [in]
OD=.6; % Specified OD of spring
Wmax=.6625; % Max width envelope for spring
N=8; % Number of turns integer
b=.625; % Fraction of turns
    
```

7

6

```

f=.15 % Friction coefficient. Lower is conservative if calculating min self-locking force
e=atan(1/(pi*f*dm));
Lockcheck=tand(y);
if f>Lockcheck
disp('self-locking')
else disp('NOT self-locking')
end
FS=1.5; % Torque Factor of Safety
Tr=((F*dm)/2)*((1+(pi*f*f*dm))/(pi*dm-(f*1)))/10*FS; % Raising Torque (Not relevant in hori
zontal) [N-cm];
Tl=((F*dm)/2)*((1-(pi*f*f*dm))/(pi*dm+(f*1)))/10*FS; % Lowering Torque (Not relevant in ho
rizontal) [N-cm];
Tavg=(Tr+Tl)/2;
steps_rev=200; % Motor characteristic
max_resolution=1/steps_rev % max resolution of screw [mm]
disp('mm')
    
```

rail_fric =
0.2000
f =
0.1500
Lockcheck =
0.1190
self-locking
max_resolution =
0.0200
mm

Y axis belt Calcs

```

clear all;
clc;
close all;
format short;
format compact;

F=10; % Force in axis desired [N]
m=10; % mass of entire axis gantry [kg]
g=9.8; % acceleration due to gravity [m/s^2]
mu=.2; % Rail friction coefficient
FS=1.5; % Y-axis factor of safety
Fa=(F+m*g*mu)*FS; % Total force required for axis including FS [N]

D=10; % Pitch diameter of 16T GT2 pulley [mm]
r=D/2/1000; % pitch radius of 16T GT2 pulley [m]
Tc=Fa*100 % Torque required at constant speed [N-cm]
disp('N-cm')

% COMPARE OUTPUTS TO TORQUE/SPEED/AMP CURVES PROVIDED AT ELECTROCRRAFT.COM
% https://www.electrocraft.com/products/stepper/TFP34/
    
```

T =

```

Angle=135; % Angle used
NB=N*nb; % Total number of turns
L1=OD*1.25; % Distance Force is applied on Leg 1
L2=OD*.25; % Distance Force is applied on Leg 2
E=28.5e6; % Material property from Table 10-5
Dpin=.125; % Pin diameter that spring is throughtmounted to
Weight=7/16*.15 %Weight of Pivot mechanism [lb]
COM=.5 %COM of pivot mechanism from pin
Nresist=0;
Mreq=Weight*COM*Mresist; % In-lb required at deployed position

Sut=A/(d^3); %Tensile strength [ksi]
Sy=.78*Sut; % Yield strength [ksi]
D=OD-d; % Mean wire diameter [in]
C=D/4; % Spring index
K1=(4*C^2-1)/(4*C*(C-1)); % Bending Stress correction factor
M=pi*d^3*Sy/(32*K1); % Max Torque
thetaC=10.8*M*D*NB/(d^4*E); % Number of turns within coil body
NB=NB*(1+thetaC)/(360*D);
k=(d^4*E)/(10.8*D^3*NB); %Spring rate [in-lb/turn]
ThetaPrime=M/k; %Max spring location [turns]
ThetaPrimeDeg=ThetaPrime*360; % Max spring location [deg]

Dprime=NB*D/(NB+thetaC); % loaded mean coil diameter
Clear=Dprime-d-Dpin; % Diametral clearance between pin and spring
Width=M*d; % Width of spring

Matowed=M*(Angle/360);
Mdeplay=M*(Angle=90)/360);

%ADD FATIGUE CALCS
if ThetaPrimeDeg<Angle
disp('UNDER ROTATE')
end
if Mdeplay>Mreq
disp('UNDER TORQUE')
end
if Matowed>M
disp('OVERSTRESS')
Overstress=Matowed-M
end
if Width>Wmax
disp('TOO WIDE')
overwidth=Width-Wmax
end
COM=3.5; % COM of moving Mechanism, origin pivot point
FS=Mdeplay/Mreq

% NOTES
% given a .875 Heater Probe, 4 inch radius. requires >=1 inch bore, prefer
% 1.125 inch bore
% given a 1.000 heater probe, 7 inch radius requires >=1.125 inch bore,
% prefer 1.25 inch bore
    
```

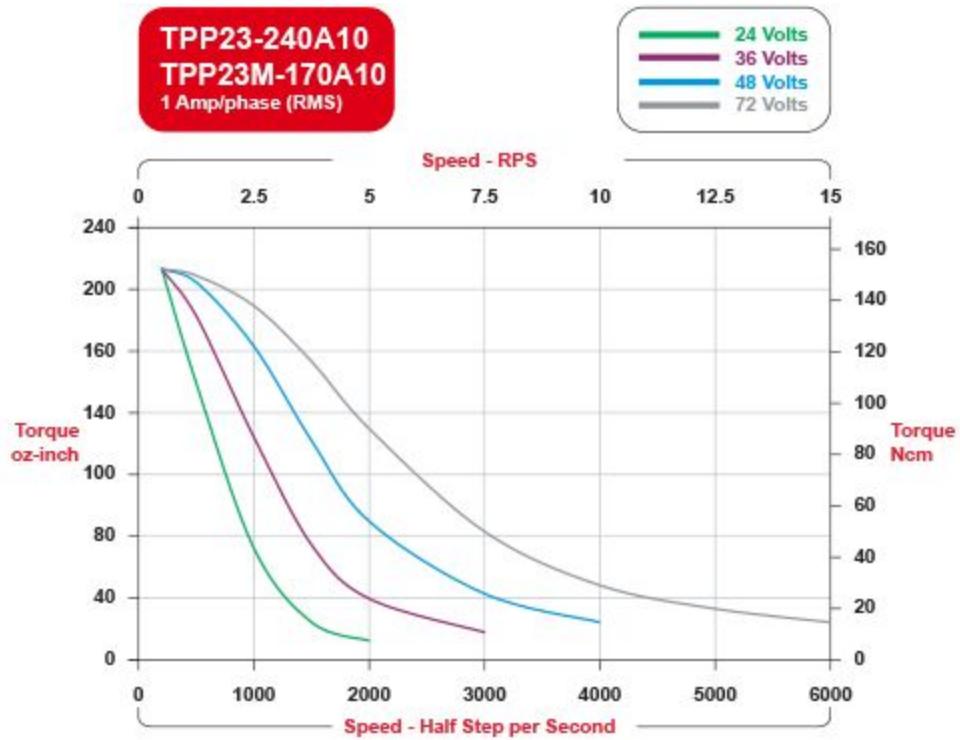
8

9

```
Weight =  
    0.5875  
CCM =  
    3.5000  
TOO WIDE  
overwidth =  
    0.1457  
FS =  
    2.0458
```

Published with MATLAB® R2019b

APPENDIX B - Lead Screw Stepper Motor Torque Curve



Torque curve for stepper motors are dependent on applied amperage and rotational speed for a given motor. STYX uses this motor at 24V, 1A. (TPP23 Stepper Motor)

APPENDIX C - Initial Drill Test Report

Test Title: Drill Rig 1, Penetration Rate and Chip Clearance

Test Date: 11/3/19

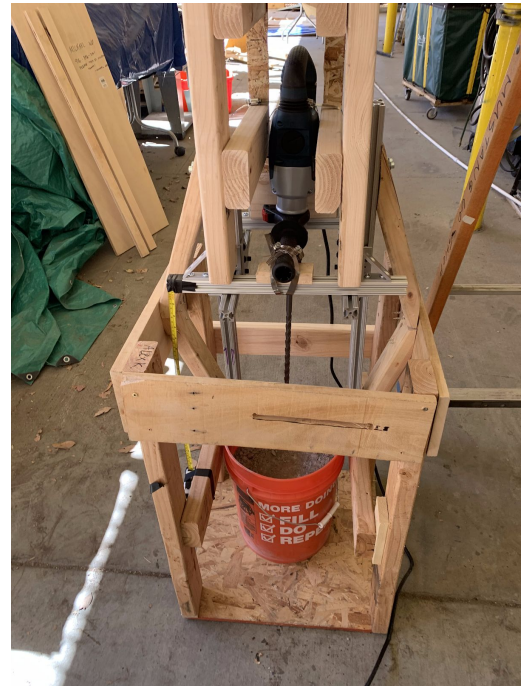
Test Goals: Verify drill function, determine maximum drill diameter, determine ideal weight on bit, test chip clearance methods, and find starting and continuous current.

Test Equipment Required:

- Hammer Drill, drill bits, and test stand
- Buckets of concrete for testing
- Safety Glasses - for ALL attendees
- Dust Masks - for ALL attendees
- (1) Face Shield
- (1) Extension cord

Test Procedure:

1. Verify all test participants are wearing proper safety equipment. These include Closed toed shoes, long pants, safety glasses, and dust masks.
2. Place Concrete bucket under test stand.
3. Mount Drill to test stand via hose clamps. Verify function via trigger.
4. Apply a constant downward force of less than 150N, and record.
5. Mark starting height of drill on frame's scale. Mark ending height (1" above bucket bottom).
6. Have stopwatch ready.
7. Test penetration rate with $\frac{1}{2}$ " , $\frac{5}{8}$ " , and $\frac{7}{8}$ " Carbide masonry bits by recording test time and depth of hole.

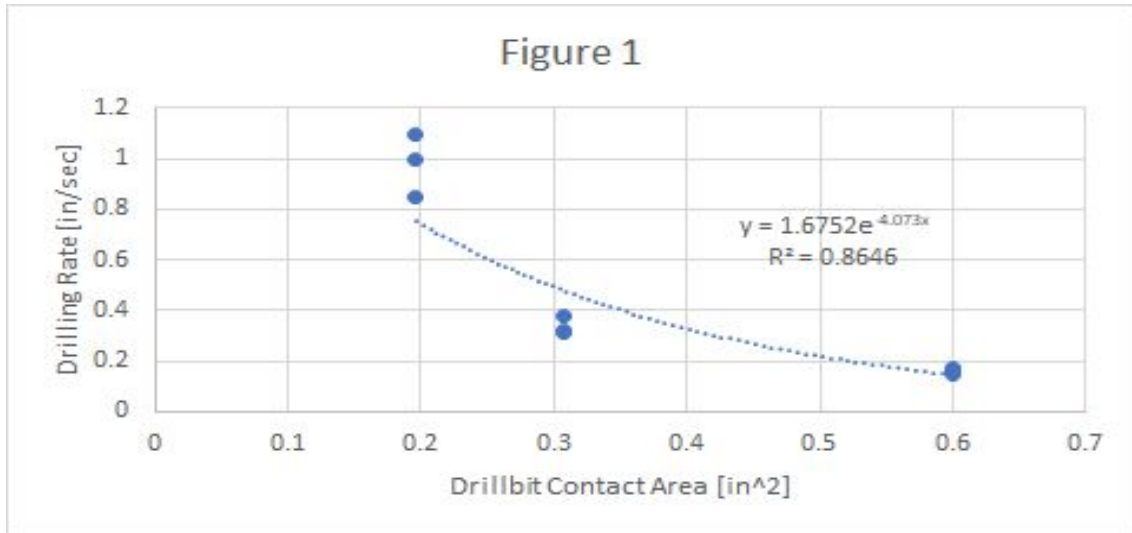


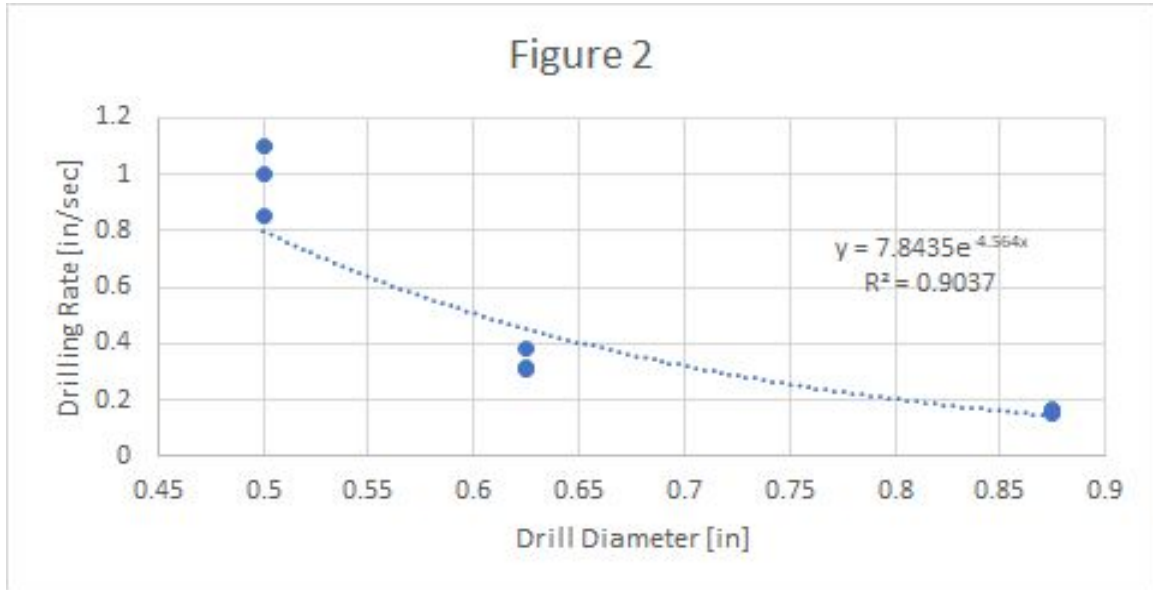
Results:

As expected, penetration rate decreased as drill bit diameter increased. Test data is recorded in Table 1. Plots comparing penetration rate and drill bit contact area and drill or drill bit diameter are reproduced as Figures 1 and 2, respectively. A stronger correlation was found between diameter and feed rate than for area and feed rate. Extrapolating this data to a 1.25" drill bit diameter results in an expected penetration rate of 1.6 inches per minute in concrete.

During testing, several tangential observations were made. Holes frequently collapsed after the drill bit was removed and typical masonry bits are not very effective at chip clearing. These issues will need to be addressed in future design considerations. Additionally, an impromptu test was conducted to test the feasibility of a pile driving mechanism. The tube was forced into a previously bored hole very easily, despite the borehole having collapsed.

TABLE 1. Drilling Test Data, 10/28/2019				
Drilling depth [in]	11			
Drill Diameter [in]	Drill Contact Area [in ²]	Trial	Drilling Time [s]	Drilling Rate [in/sec]
0.5	0.196	1	10	1.1
0.5	0.196	2	11	1
0.5	0.196	3	13	0.85
1/2" Average			11	0.98
0.625	0.307	1	36	0.31
0.625	0.307	2	29	0.38
0.625	0.307	3	34	0.32
5/8" Average			33	0.34
0.875	0.601	1	66	0.17
0.875	0.601	2	72	0.15
0.875	0.601	3	70	0.16
7/8" Average			69	0.16





APPENDIX D - Filtration Test Report

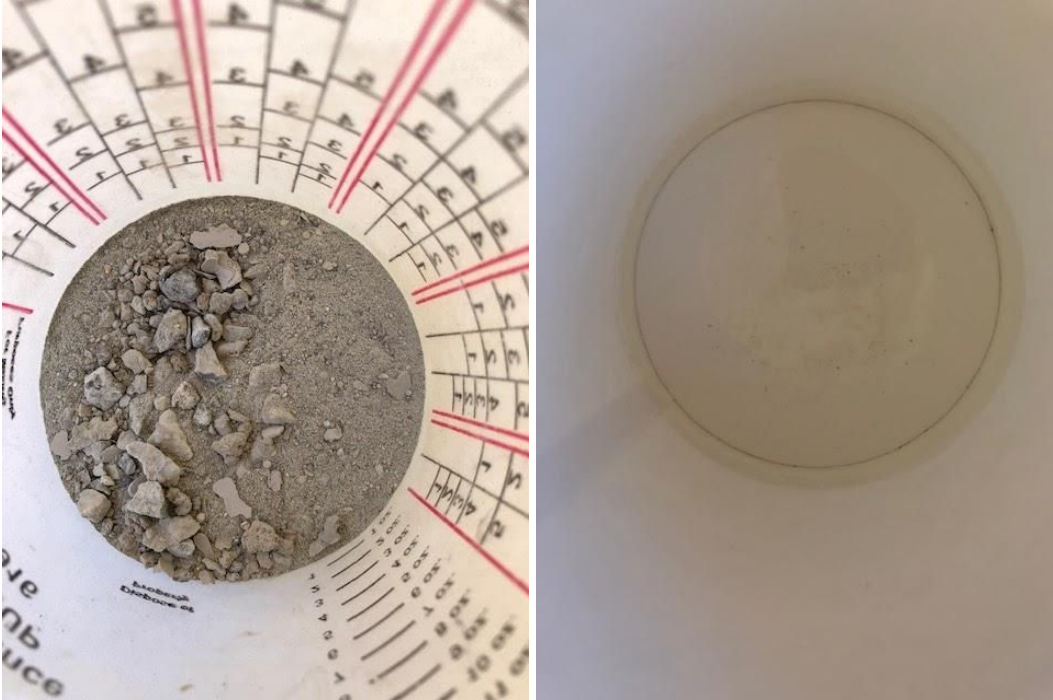
Test Procedure:

1. Wear a dust mask while moving the dry contaminants.
2. Prep the contaminated water samples. Start by adding 1 oz of solid material to a measuring cup, and top off with water to the 16 oz line. Concrete powder taken from previous drilling tests will be used in test 1. Test 2 will be repeated with sand.
3. Place the water sample at an elevation of 2 ft above the filter and prime the siphon.
4. After all the water flows through the filter, disassemble the filter to observe how obstructed the filter material has become, and note the amount of sediment left in the bottom.
5. Perform a visual check on clarity and sediment in the filter output.

Test Results

During the first test, the team came across two major problems. First, large pieces of broken concrete (dia > 1/8") constantly created blockages at the intake. Second, concrete powder tended to coagulate when subjected to liquid water. This phenomenon caused blockages throughout the intake tube. Although this first test was stopped before completion due to the constant clogging, the test yielded valuable data. The 20 micron filter was sufficient enough to produce clear water. For the next test, the team will increase the intake line to 1/4", and implement a coarse screen at the inlet to avoid having large solids clog the tube.

In the second test, the particles of sand passed into the filter without causing a backup. The sediment trap design worked well, as all of the course sand settled out below the suspended filter. This data ensures the team that the filter will not become quickly impacted by large material. However, the sand had a lot of fine particulate within it, and after the test, roughly 50% of the filter surface area (2 in²) was covered in fine particulate. This means that filter surface area will have to be increased to avoid backflushing the system too often. Also, the water output was visibly darker in this sample. The team was not satisfied with the final water clarity. The next step will involve testing a 5 micron filter for output clarity.

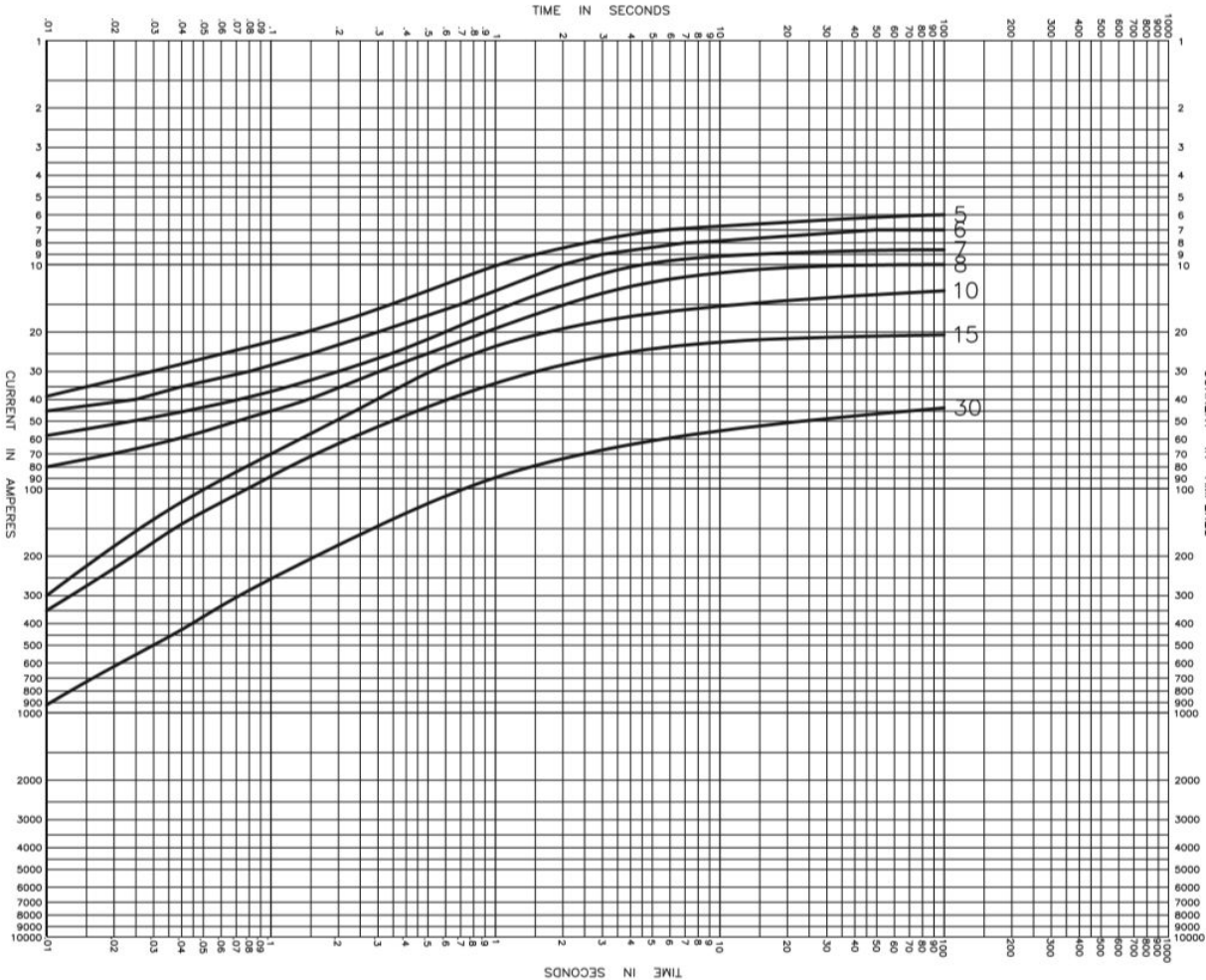


Test 1 : Dry concrete sample prepared for test (left), final filtered water (right)



Test 2 : Sand sample prepared for test (left), final filtered water(right)

APPENDIX E - Fuse Amp-Time Curve

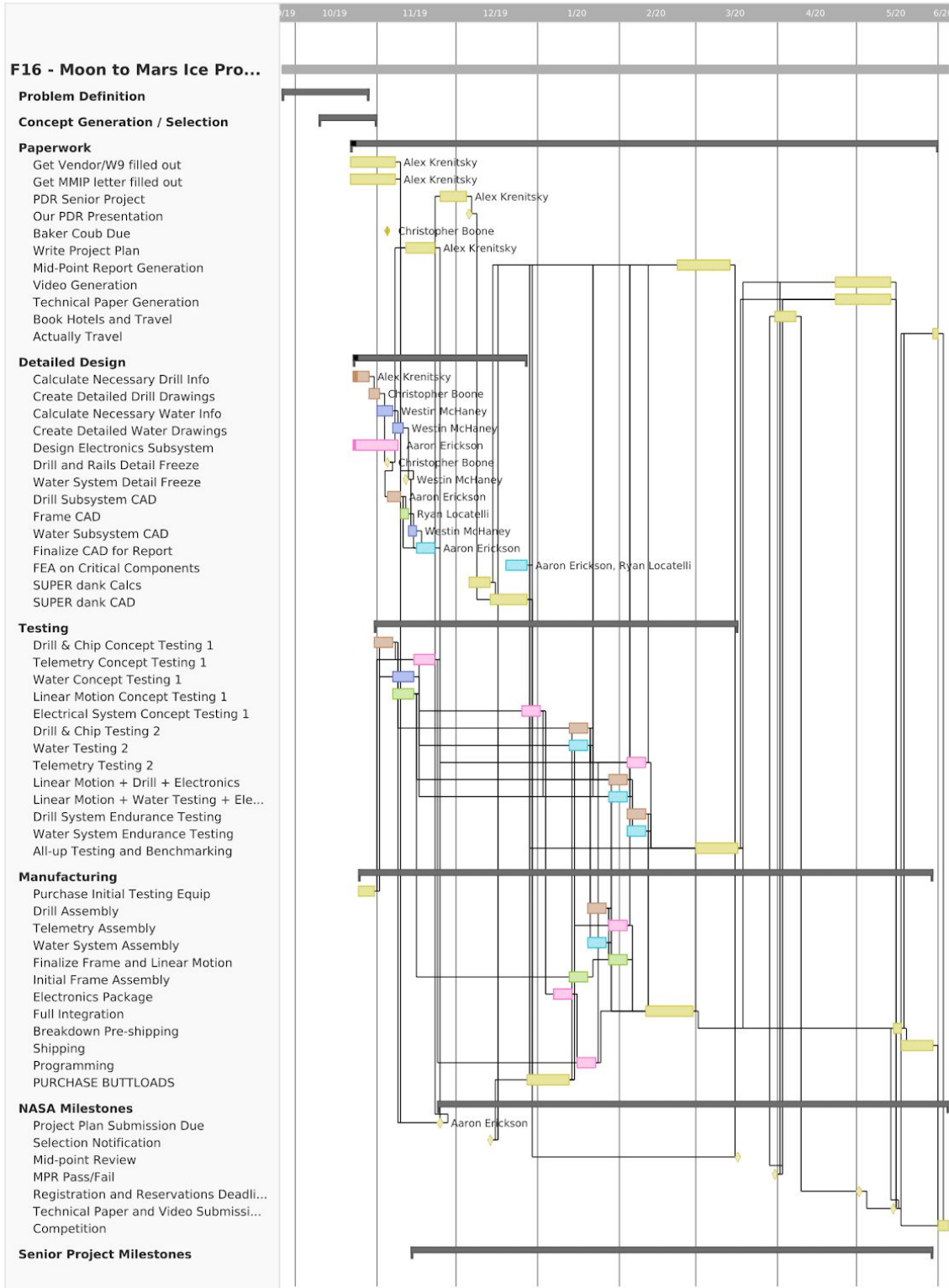


Maximum current curve for the Bussman BK/AGC-9-R Fuse (Bussmann Series TDS).

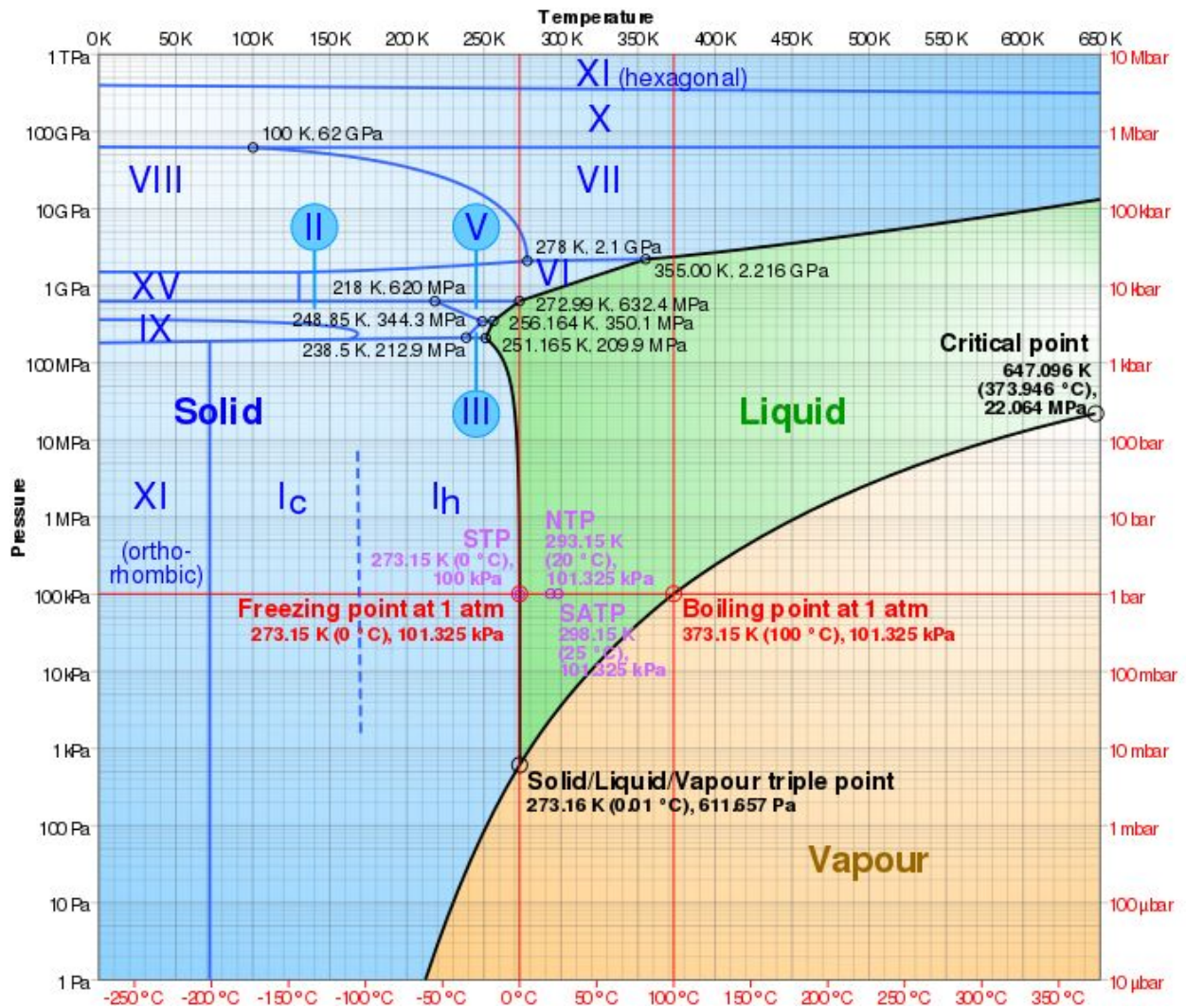
APPENDIX F - Component Power Budget

ALL SYSTEMS					
Subsystem	Component	Operating Voltage [V]	Operating Current [A]	Conversion Efficiency	Power (W)
Drilling	Drill	120	8.5	1	1020
	Induction Coil Heater	24	30	0.85	847
Axis Motion	X-Axis Stepper	24	2	0.85	56
	Z-Axis Stepper	24	2	0.85	56
	Rotary Stepper	5	2	0.85	12
Heating	Heater	120	7.5	1	900
	Heater Stepper A	5	3	0.85	18
	Heater Stepper B	5	3	0.85	18
Extraction	Pump	12	1	0.85	14
Control	Arduino	12	0.5	0.85	7
	Cameras	12	0.5	0.85	7
	DAQ Amplifiers	12	0.5	0.85	7
	Servos	5	1	0.85	6

APPENDIX G - Project Gantt Chart



APPENDIX H - Triple Point Curve of Water



This is a pressure-temperature phase diagram for water. This was used when analyzing the validity of the design choices that would be implemented on Mars (Chaplan, Martin).

APPENDIX J - Background Research and Project Outline

Alex Krenitsky
akrenits@calpoly.edu

Aaron Erickson
aberickson101@gmail.com

Chris Boone
cbboone1197@gmail.com

Ryan Locatelli
rlocatel@calpoly.edu

Westin McHaney
westincello@gmail.com

Mechanical Engineering Department
California Polytechnic State University
San Luis Obispo
Fall 2019

PREPARED FOR:
Peter Schuster, Project Advisor

1.0 Introduction

Recent discoveries of what are thought to be large ice deposits under both lunar and Martian surfaces have mission planners re-thinking how sustained human presence on the Moon and/or Mars could be enabled by a “water rich” environment. Water is essential to enabling a sustained presence, as it could enable agriculture and propellant production, reduce recycling needs for oxygen, and provide abundant hydrogen for the development of plastics and other in-situ manufactured materials. Before the water can be used to support sustained human presence, it must be extracted from the ice deposits. However, getting to the water will be a formidable task due the variety surface material layers that can be encountered on top of that ice. The composition, density, and hardness of each of these layers presents different drilling challenges, and it is crucial that we develop systems that can identify different layers and understand what modifications need to be made to mine through them in order to reach the ice. The purpose of this challenge is to demonstrate methods to identify different layers using system telemetry and extract water from lunar or Martian ice deposits.

Participating team members take on the role of astronauts who monitor and control drilling operations. Using a combination of remote control and hands-off operations, teams will extract as much water as possible from the buried ice in a simulated lunar environment. In order to demonstrate a wide range of capabilities of interest to exploration and science, team member interaction with the prototype will be divided into a period where “hands-on” operation and repairs are permitted and a period where physical “hands-off” operations will take place. During all phases of the competition, the teams will be able to use a control system to “remotely” operate the water extraction system. (1)

Contained in this document is a background section, detailing the research completed by each subsystem, an objectives section, detailing the system boundary and requirements, and a project management section, which describes our plan for completing objectives on a timeline.

2.0 Background

During the initial research phase of this project, we focused on gathering and quantifying the RASC-AL competition requirements listed on the NASA website. Research topics include drilling methods, telemetry, and ice extraction. The drilling team looked into industrial drilling for inspiration and information on drill head types and chip clearing methods. The telemetry team called a local drilling company and discussed the pros and cons of gamma ray detection as well as tactile sensing, to be used to map out the ground composition under the drill. The ice extraction team, looked at electrical and liquid heating systems available for ice extraction. Additionally, some members of the team were specifically tasked with reviewing competition footage from previous years to identify common solutions and areas for improvement.

For researching ways in which NASA has already tried to solve the problem at hand, the team was given access to 19 sources such as scientific journals and various experimental results published by NASA. These resources cover topics such as information on NASA’s Icebreaker

Drill, test data on enhancing cuttings removal methods, and an analysis of a drilling procedure that took place on Mars (2).

2.1 Telemetry Team

The telemetry team identified several viable means of collecting data on the regolith layers presented to us at competition. Two main methods were identified through discussions with companies in industry, gamma concentration and resistivity. Gamma concentration requires dropping a Gamma sensor down the bore hole and measuring the amount of gamma radiation given off by each layer (3). This value would be compared to a list of known materials for identification. Resistivity measuring requires characterization of the electrical or natural frequency properties of the regolith layers for comparison to a list of known materials (4). The gamma concentration method is not yet accurate enough to separate for the short layer heights used in this competition. The resistivity method would require exceptionally expensive equipment and a lot more testing to ensure reliability in our implementation (5). Additionally, neither of these methods gives us the exact data type we are seeking. Compressive strength would have to be extrapolated from the type of rock we believed we had identified.

As a result of these challenges, we will likely default to the simpler approach of correlating downwards pressure with feed rate to determine the compressive strength of each layer. This method was used effectively by winning teams in the past and several improvements can be made to the system to reduce noise and increase accuracy. These improvements include taking measurements without a percussive action being used and using a smaller, flat-ended drill bit to accurately measure the amount of pressure being applied to the layer in question.

2.2 Drill Team

The drill team made significant progress towards identifying effective drilling systems available to us, given the low axial force and power allowances. Three methods of drilling were identified as plausible for this competition: rotary drilling, percussive rotary drilling, and ultrasonic drilling. Chip removal was also identified as a huge factor in the efficacy of any drilling system. "Drilling in Extreme Environments" includes information about the three types of drills previously mentioned, and goes into detail about how they could be used on the surface of the moon or Mars (6). Drill bit selection is currently tabled for near-future research and discussion, once a drilling method is decided.

Rotary drilling as a method has only one possible benefit over the other methods. Telemetry data with a drill bit that is not being actuated percussively would be significantly less noisy. The drawbacks of this method are numerous given the project constraints, however. Rotary drilling requires significant axial force to cut through hard materials. With the force maximum of 150N, drill bit wear would be a significant issue. Some studies found a reduction in penetration rate of 50% in under 2 minutes when drilling harder materials with low axial force (7). Rotary drilling also makes drill bits freezing into the icy underlayer a significant issue, as any reduction in downwards pressure will allow for the ice to refreeze, capturing the drill bit in the process.

Percussive rotary drilling is currently identified as the most viable candidate for drilling method. The percussive action is capable of breaking up harder materials when combined with the correct drill bit and the rotary action is effective for softer dirt and will aid significantly with chip

removal. Winning teams of previous years have used this drilling method with great success. The only disadvantage of percussive rotary drilling is that the frequency of percussion is lower than optimal, with some higher end models of hammer drills only reaching about 10Hz. Vibrations with a frequency of 50Hz or greater show greatly improved soil penetration and chip removal abilities, as the soil exhibits fluidic properties at these higher frequencies (6).

Ultrasonic drilling is an area of ongoing research for JPL and NASA. Drilling into rock with frequencies in excess of 20kHz has a significant effect for harder materials. This method uses almost no axial force (~10N) and very little power (100W). Penetration rate has been shown to be viable as well, with the MIDAS project reaching a penetration rate of 120cm/hr through simulated martian soil (6). There are no economically viable commercial units available for the drilling depth the project requires, but there is ample resources available to design a custom apparatus, likely constructed from components used in industrial-grade ultrasonic cleaners. Chip removal remains a problem, but compressed air has been identified as an effective solution. The non-rotating method of cutting is also capable of coring small diameter holes effectively.

In the rotary drilling category auger drilling is a viable option. The augers lift chips up and out of the hole as it is drilled allowing for more time to be spent on drilling, and not evacuating chips from the hole. Auger drills can be configured to bore through rock, as shown in Figure 2, allowing us to have the capability to bore through the toughest overburden layer.

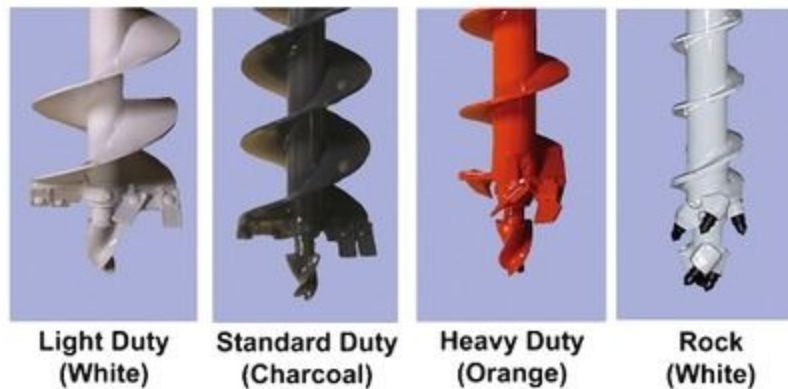


Figure 1: Auger Drill types (a)

Another rotary drilling type is coring drills. These drills allow for faster drilling due to reduced contact area, however most of the time is spent evacuating the core from the drill. Diamond coring heads allow holes to be bored through very hard rock layers; Figure 2 displays the variety in diamond coring bits available. Additionally most diamond coring bits are larger than 1" in diameter, providing our team more room for water extraction, but increasing drilling time by expanding the hole size.



Figure 2: Diamond Coring (b)

2.3 Ice Extraction Team

The ice extraction team, selected different options for water pumping and ice melting. For the ice melting process, both a thermal storage system and a direct electrical heating systems were compared. Looking to simplify the device as much as possible, to reduce chances of error, a direct electrical heating element was chosen. Many types of heating elements and their data sheets are available on the Tempco website, an electric heating corporation based in Illinois(8). The next thing researched by the ice extraction team was, methods of pumping water from the bottom of the drill hole. There are large particulates in the water extracted from the bottom of the hole, so the pump will need to be able to handle the load. The solution to this is using a peristaltic pump, this works by mashing a flexible tube to create a low pressure at the pump inlet, there are not any moving parts that are in contact with the fluid so the pump will not get blocked by particulates.

Another option remains in which the drilling mechanism also serves as the water extractor. One such method described by Honeybee Robotics (9), is the “sniffer”. This device functions similarly to a natural gas extraction unit. A fluted auger with holes is used to drill into an ice rich area. Heaters within the auger are then used to sublimate the ice, where it is collected through the holes in the auger and ran through a cold trap on the surface. Another option presented is a deep-fluted auger that retracts into a heated cylinder where ice is converted to a gas and extracted. The third option presented is a dual-wall coring auger. Here, the ice is heated and extracted while the drill continues, in order to be more time efficient. Tests were done on these three systems. The sniffer was not consistently able to extract water. Vapor sublimed but ultimately did not enter the auger. Both of the two remaining auger systems were able to extract ice. Tests results show that smaller diameter augers are more energy efficient and they could capture a larger percentage of the sublimated ice. The biggest problem with the coring device is that it is difficult to control the ability to hold a core sample, and extract the remaining solid after the ice is extracted. Ultimately, coring bits outperformed augers in both ground penetration rate and energy consumption.

Table 1: Relevant Patents

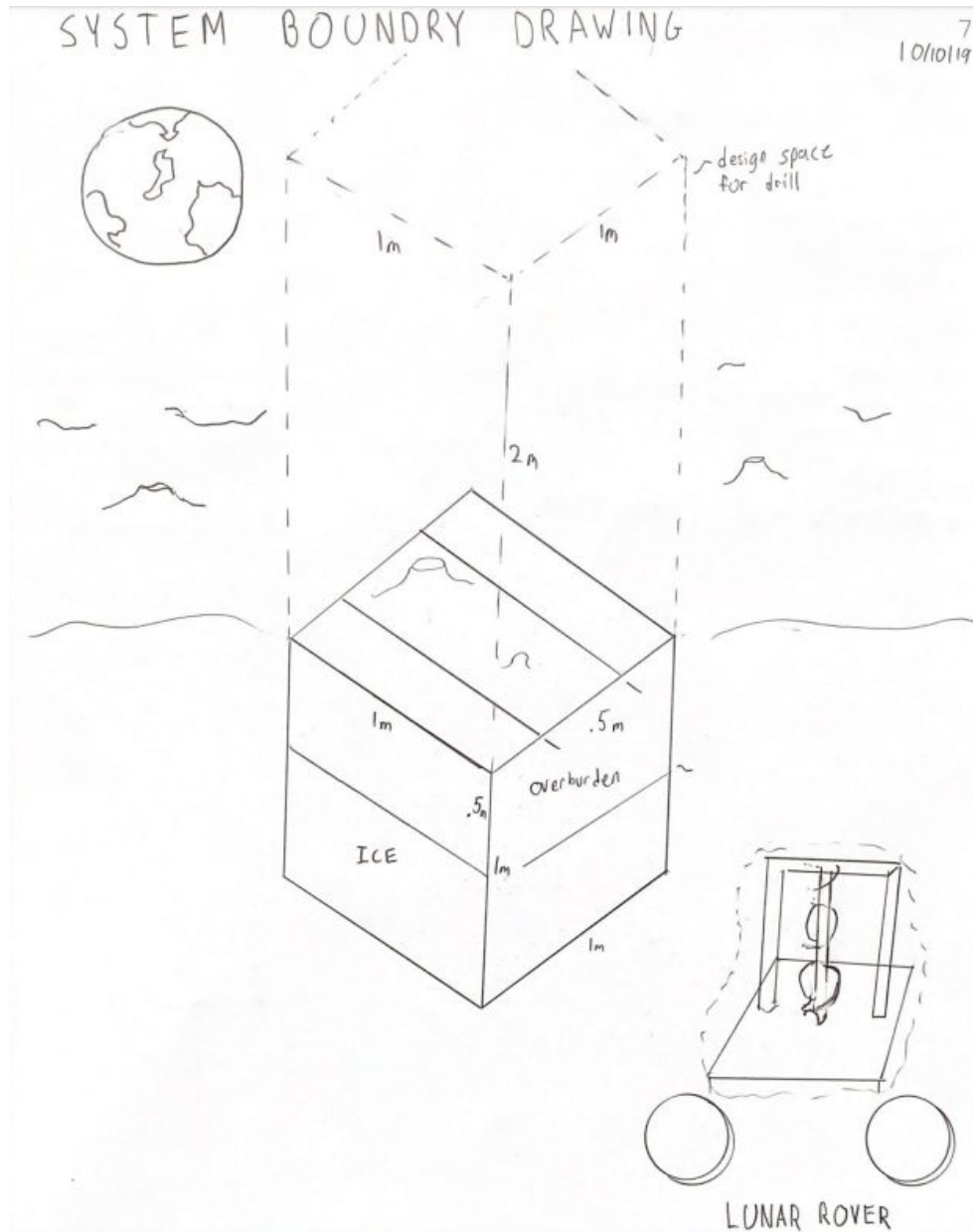
Patent Number	Patent Name	Description
---------------	-------------	-------------

US8038630B2	Floating Probe for Ultrasonic Transducers	The invention is a novel device with an ultrasonic based drill and corer. The invention uses ultrasonic vibrations, which are produced by a frequency compensation coupler, to produce a hammering action with a relatively low axial-force.
WO2001083933A1	Smart-ultrasonic/sonic driller/corer	This invention is a concept for an ultrasonic based drill and corer. This iteration uses a free mass that vibrates back and forth to transfer the vibratory force to the bit, rather than having the bit directly affixed to the piezoelectric transducer.
US7578662B1	Peristaltic Pump	A peristaltic roller pump that includes a rotor carrying a pumping roller on one end and an occluding roller on the other end. Occluding roller is designed to not cause any pumping of fluid through the section of the tubing under that roller. This is a low power, low flow pump that can move liquids with high particulate concentrations.
US6550549B2	Core Break-off Mechanism	A mechanism for breaking off and retaining a core sample from a drill drilled into the ground. This device utilized two offset cores, that when spun relative to each other, create an offset that breaks the desired core from the ground, allowing the sample inside of the coring bit to be brought out of the bore hole.
CN203264409	Low-pressure self-cleaning continuous filter	The low-pressure self-cleaning continuous filter is simple in structure, self cleans the filter, low in cost, and capable of uninterrupted filtration.

3.0 Objectives

- Create a digital core using telemetry
- Mine through various overburden layers
- Extract clean liquid water
- Teams need to design and bring water transfer equipment (at least 3 meters)
- Design needs to work in long term (ie. backflushing filters)

3.1 System Boundary Diagram



4.0 Project Management

To achieve a coordinated, concentrated effort on a project with such a large scope, we will be splitting our team of 5 into sub-teams each week based on workload. As an example, thus far we have been split into a drill team and a water collection team. This division allowed for more concentrated research efforts and therefore better informed decisions regarding subsystems. To ensure the workload is fully accounted for and we are concentrating on the most time-efficient items, weekly meetings are called outside of class to discuss progress and redirect efforts if necessary. Additionally, critical project management roles have been identified and assigned to individual team members. These roles are: project scheduler, budget and purchasing, NASA communications, and Weekly Status Report Lead.

4.1 Software and Data Solution

To maintain consistency in file creation in storage, our software solutions will be google drive, Solidworks 2019, MATLAB 2019, and TeamGantt. If the CAD files generated consume too much space on google drive, our team will pivot to Microsoft OneDrive as the primary storage solution. We will be updating our TeamGantt timetable frequently to keep our progress on track moving toward tight, upcoming deadlines. The current Gantt chart is attached in appendix A.

4.2 Next Steps and Prototyping

The first NASA-imposed milestone is submission of our design and associated research by November 24. To get started on detail design as early as possible, we are self-imposing a concept-freeze on October 24. Prototyping will begin immediately following notification of our selection status. To manage prototyping and testing of such a complex system, we plan to build top-down and test/iterate subsystems along the way. As an example, the drilling sub-team will purchase the drill, benchmark/ensure adequate performance, build the linear motion system and test for structural rigidity in a real use-case before integrating into the frame and water collection system. We anticipate the prototyping process to be quick and very iterative as we discover challenges not yet known. We identify this stage to be one of the largest sources of risk in our projects, as most teams will be returning and have prior knowledge and experience regarding the competition environment. Additionally, to facilitate such a fast-paced schedule in the early days of the project, ME 428 requirements are being relaxed in certain areas. The specificity of the project requirements and customer needs allows for certain early ME 428 deliverables to be reduced in scope or omitted to ensure time is being spent appropriately. These revised deliverable expectations will be carefully tracked and discussed with the project advisor on a weekly, ongoing basis.

Table 2: Timeline of deliverables for competition.

Dates (Eastern time 11:59 pm)	Description
November 24, 2019	Project Plan submission deadline
December 13, 2019	Teams are notified of their selection status
Late-December, 2019	1st installment of development stipend sent to universities
March 15, 2020	Mid-Point Review deadline
March 30, 2020	Teams are notified of MPR pass/fail status and stipends are sent to universities (as appropriate)

May 1, 2020	Deadline for Hotel Reservations
May 1, 2020	Online registration and payment deadline for the Forum
May 14, 2020	Technical Paper and Integration Document submission deadline

Conclusion

The team will be designing a system to drill through hard layers of regolith simulant, extract water, and purify water to a drinkable standard. The largest hurdle for the project will be submitting a detailed design paper by the November 24th deadline. To manage workload in the upcoming weeks, significant tasks will be continually updated in our team's gantt chart. We are expediting the concept generation process to begin the detailed design and CAD work required as soon as possible. If selected by NASA to compete, the project will be moving at a more manageable pace through prototyping and testing.

Works Cited

- (1) "Competition Basics: RASCAL-AL Special Edition." *RASCAL-Challenge*, NASA, 2019, specialedition.rascal.nianet.org/competition-basics/.
- (2) "Resources: Recommended Reading" *RASCAL-Challenge*, NASA, 2019, specialedition.rascal.nianet.org/resources
- (3) "Gamma Radiation Sensors." *Gamma Radiation Sensors | RAE Systems*, www.raesystems.com/solutions/gamma-radiation-sensors.
- (4) "Resistivity Logging." *Halliburton*, www.halliburton.com/en-US/ps/sperry/drilling/logging-while-drilling/resistivity-logging/default.html?seq=13
- (5) "API Natural Gamma Ray." *Scientific Drilling*, scientificdrilling.com/technology-services/logging-while-drilling/sci-gamma/
- (6) Bar-Cohen, Yoseph, et al. *Drilling in Extreme Environments: Penetration and Sampling on Earth and Other Planets*. Wiley-VCH, 2009.
- (7) Zacny, K., et al. "Drilling systems for extraterrestrial subsurface exploration." *Astrobiology*, vol. 8, no. 3, 2008, p. 665+. Gale Academic Onefile, Accessed 17 Oct. 2019.
- (8) Tempco Corporation. "Electric Heaters and Elements." *Tempco*, www.tempco.com/Tempco.htm.
- (9) Honeybee Robotics. "Planetary Volatiles Extractor for In Situ Resource Utilization." <http://rascal.nianet.org/wp-content/uploads/2016/08/PVEx-for-ISRU.pdf>
- (10) "Augers Information." *Engineering 360*, IEEE, Jan. 2010, www.globalspec.com/learnmore/building_construction/building_construction_tools_machines/augers.
- (11) "Drilling Rig." *Wikipedia*, Wikimedia Foundation, 2 Oct. 2019, en.wikipedia.org/wiki/Drilling_rig.
- (12) Obermeier, Josef. *Rock Drill with Conveying Groove*. 30 Jan. 1996.
- (13) Benchoff, Brian, et al. "A Very Tiny Gamma Ray Detector." *Hackaday*, 3 June 2013, hackaday.com/2013/06/03/a-very-tiny-gamma-ray-detector/.

- (14) Xie, et al. "Value of 20Mhz NMR Core Analysis for Unconventional Mudstones." *OnePetro*, Society of Petrophysicists and Well-Log Analysts, 2 June 2018, www.onepetro.org/conference-paper/SPWLA-2018-FFFF.
- (15) "SEG Library." *SEG Library*, library.seg.org/.
- (16) S., Michael, et al. "A New Azimuthal Deep-Reading Resistivity Tool for Geosteering and Advanced Formation Evaluation." *SPE Reservoir Evaluation & Engineering*, Society of Petroleum Engineers, 1 Apr. 2009, www.onepetro.org/journal-paper/SPE-109971-PA.
- (17) "US7253401B2 - Spectral Gamma Ray Logging-While-Drilling System." *Google Patents*, Google, patents.google.com/patent/US7253401B2/en.
- (18) "US4698501A - System for Simultaneous Gamma-Gamma Formation Density Logging While Drilling." *Google Patents*, Google, patents.google.com/patent/US4698501A/en.
- (19) "US6377050B1 - LWD Resistivity Device with Inner Transmitters and Outer Receivers, and Azimuthal Sensitivity." *Google Patents*, Google, patents.google.com/patent/US6377050B1/en.
- (20) Bar-Cohen, Yosef, et al. "Ultrasonic/Sonic Mechanisms for Drilling and Coring." NASA, NASA's Jet Propulsion Laboratory, Sept. 2003
- (21) Damadeo, Kristyn. "West Virginia University Takes Top Prize in Moon to Mars Ice Challenge." NASA, NASA, 7 June 2019, www.nasa.gov/feature/west-virginia-university-takes-top-prize-in-nasa-test-of-concepts-to-extract-water-on-the.
- (22) Hamilton, Charles, and Gary Wayne Hamilton. *Rock Auger Drill Patent*. 16 Sept. 2003.
- (23) Kollé, J.J. "The Effects of Pressure and Rotary Speed on the Drag Bit Drilling Strength of Deep Formations." *SPE Annual Technical Conference and Exhibition*, 1996, doi:10.2118/36434-ms.
- (24) Liu, Songyong, et al. "Drilling Performance of Rock Drill by High-Pressure Water Jet under Different Configuration Modes." *Shock and Vibration*, vol. 2017, 2017, pp. 1–14., doi:10.1155/2017/5413823.